Article:
Liang, G, Zeng, Y, Hu, X et al. (7 more authors) (2017) Monolithic semiconductor lasers with dynamically tunable linear-to-circular polarization. ACS Photonics, 4 (3). pp. 517-524. ISSN 2330-4022

https://doi.org/10.1021/acsphotonics.6b00703

Supplementary Information for

Monolithic semiconductor lasers with dynamically tunable linear-to-circular polarization

Guozhen Liang,[1] Yongquan Zeng,[1] Xiaonan Hu,[1] Hao Yu,[1] Houkun Liang[2], Ying Zhang[2], Lianhe Li,[3] Alexander Giles Davies,[3] Edmund H. Linfield,[3] Qi Jie Wang[1,*]

[1] *Center for OptoElectronics and Biophotonics, School of Electrical and Electronic Engineering & The Photonics Institute, Nanyang Technological University, 50 Nanyang Avenue, 639798 Singapore.*

[2]*Singapore Institute of Manufacturing Technology, 71 Nanyang Drive, 638075 Singapore.*

[3]*School of Electronic and Electrical Engineering, University of Leeds, Leeds LS2 9JT, UK.*

**Email: qjwang@ntu.edu.sg*

1. Light-current-voltage (LIV) characteristic, and spectrum, of the QCL

Fig. S1 shows the light-current-voltage (LIV) characteristic, and spectrum, of the right QCL at 10 K. The left QCL shows similar LIV curves, and a spectrum that is only slightly modified. The devices operate up to 120 K under pulse mode operation (500 ns pulse width, 10 kHz repetition rate), which is comparable to that of a conventional (double-metal waveguide) ridge laser fabricated from the same QCL wafer, which had a maximum operating temperature of 136 K under the same operating conditions.

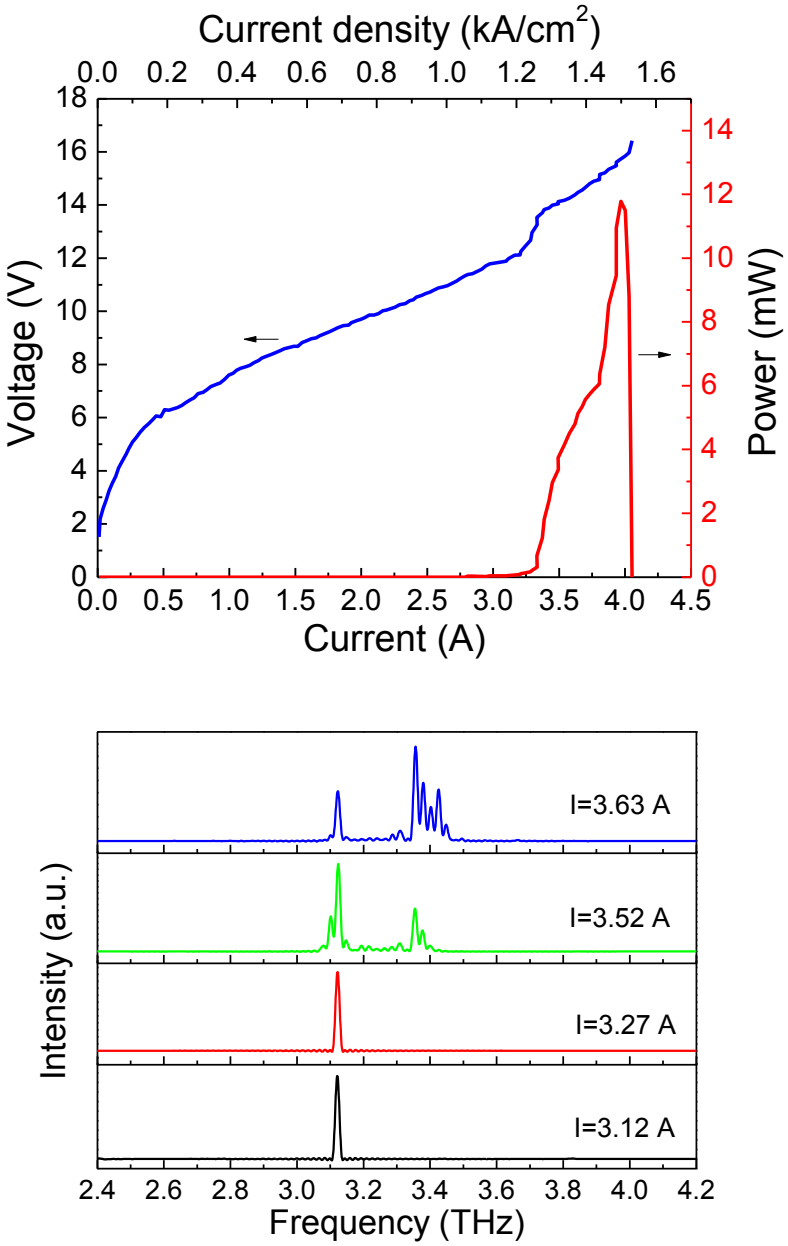

Figure S1. (a) Light-current-voltage characterization of the right hand QCL at 10 K. (b) Spectra of the device with increasing current.

2. Selection of the antenna dimensions and lateral separation

The dimensions of the antennas are chosen to let the antennas resonate at the targeted frequency (~3.0 THz) so as to strengthen their scattering efficiency. The resonance frequency is mainly determined by the length and width of the antenna. The effect of the thickness is minor as it varies from 200 nm to 500 nm, so it is let the same as the thickness of the top contact of the laser (~400 nm) so that the antennas and the laser contact can be deposited at the same time in fabrication (Fig. S3(c)). To suppress the electric field component polarized perpendicular to the antenna length, the width should be kept as narrow as possible. However, considering the micro-fabrication limitations and to allow for some fabrication tolerance, we chose a width of 3 μm. The length of the antenna was then determined to be 21 μm assisted by FDTD simulations (Fig. S2(a)). As for the lateral separation, it should be large enough to avoid the coupling between adjacent antennas, i.e., the electric field of a certain antenna will not be interfered by the adjacent ones. Fig. S2(b) shows the antenna resonances with various lateral separations. The shift of the resonant peak around 3.0 THz is due to the coupling of the adjacent antennas for the lateral separation smaller than 37 μm. When the separation is larger than 37 μm, the antenna resonant peak is unaffected, indicating that the adjacent antennas are not coupled anymore. Note that for the second resonant peak around 4.1 THz, which corresponds to the resonance in the GaAs pedestal, it is shifting even for lateral separation larger than 37 μm. This is because this resonant mode is more spatially extended (lower right inset in Fig. S2(a)).

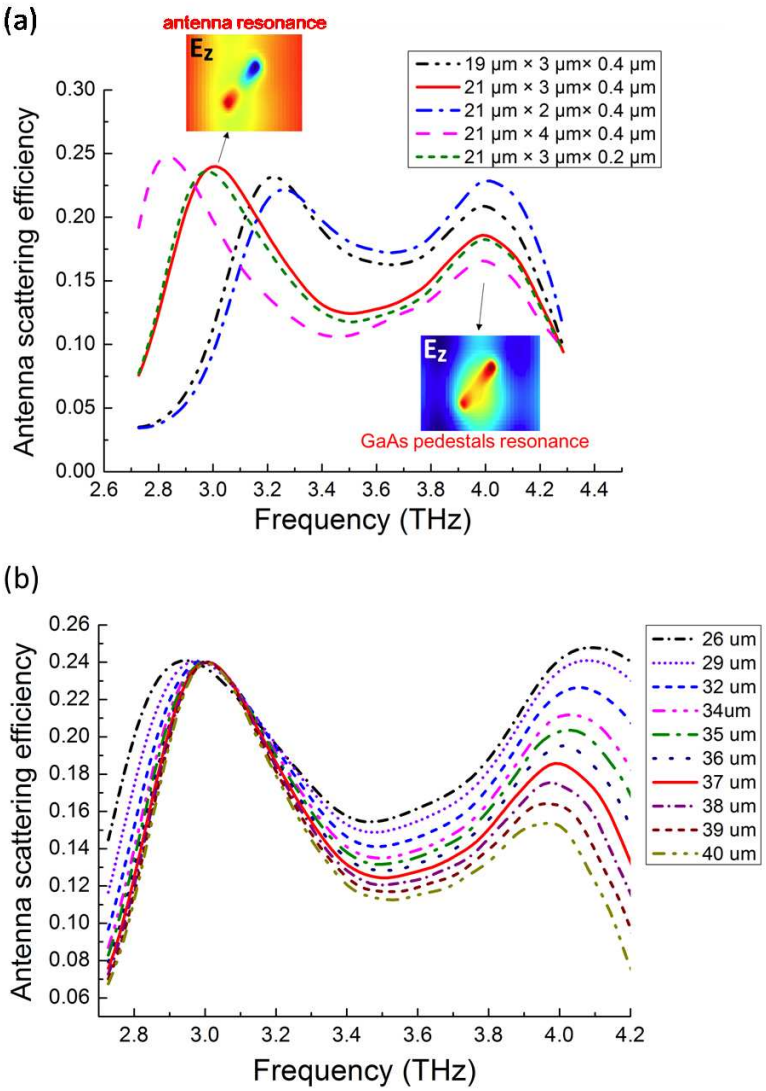

Figure S2. (a) The scattering efficiency of the antennas with different dimensions. The red solid line corresponds to the design in our work, which has a resonant frequency at ~3.0 THz. The first peak in the curves corresponds to the antenna dipole resonance, which will produce a linearly polarized light, while the second peak is related to the resonance in the underneath GaAs pedestal, which is not desirable. (b) The resonance of the antennas with various lateral separations. The shift of the resonant peak around 3.0 THz is due to the coupling of the adjacent antennas for lateral separations smaller than 37 μm. When the separation is larger than 37μm, the antenna resonant peak is unaffected, indicating that the adjacent antennas are not coupled anymore.

3. Coupling efficiency of the half racetrack structure

Fig. S3(a) shows the Finite-difference time-domain (FDTD) simulation configuration of the half racetrack structure. Approximately, for the THz light injected from the upper right port,

~60% of the light will be reflected back by the gap, ~10% will be coupled into the half racetrack structure, with the remaining being scattered out. Finally, ~1% of the light will be injected into the lower right port, after propagating through the half racetrack structure. The specific values of the reflection and injection efficiency is frequency-dependent, as shown in Fig. S3(b).

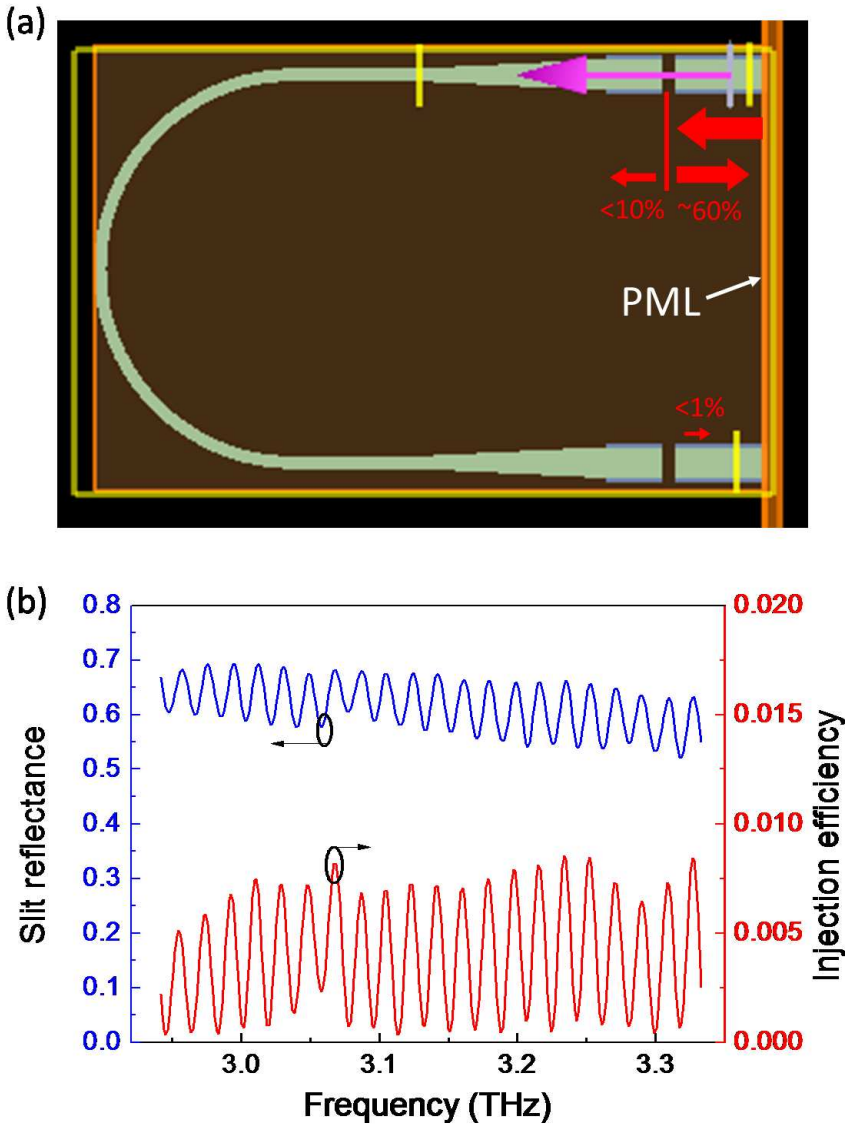

Figure S3. (a) FDTD simulation configuration of the half racetrack structure, the THz light is injected from the upper right port. The simulation domain is surrounded by perfectly matched layers (PML) to absorb any outgoing light. (b) The calculated slit reflectance (left axis) and the percentage of light injected into the other laser (right axis).

4. Relatively independent control of the intensity from each laser

As the coupling is relatively weak (1% injection efficiency compared to the 60% reflectance of the gap), the amplitude of each laser can be tuned quite independently. Fig. S4 presents the measured optical power of the device passing through a wire-grid polarizer as a function of the injection current to the left QCL, while fixing the current of the right QCL at 3.68 A (Fig. S4(a)) and 3.95 A (Fig. S4(b)). The black curves correspond to the cases when the polarizer is at 45º so that mainly the light from the right QCL can pass through the polarizer. The red curves correspond to the cases when the polarizer is at 45º and mainly the light from the left QCL can pass through. As it is shown, when changing the current of the left QCL, the powers from the right QCL (black curves) remain relatively unchanged. Therefore, the ratio of the amplitude from the left and right QCL can be freely tuned so that the polarization of the resulting beam is widely tunable.

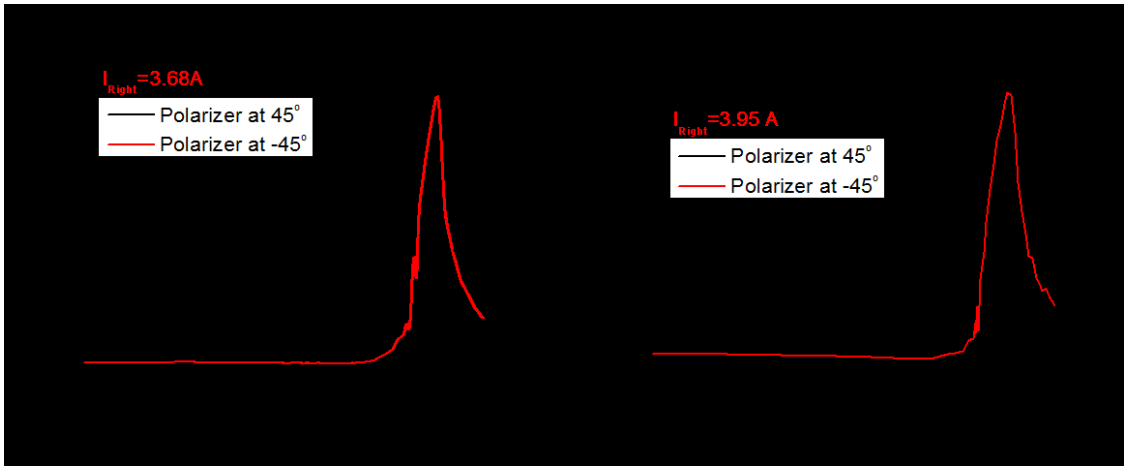

Figure S4. The measured optical powers of the device through a wire-grid polarizer as a function of the injection current to the left QCL, while fixing the current of the right QCL at 3.68 A (a), and 3.95 A (b). The black curves correspond to the cases when the polarizer is at 45º so that mainly the light from the right QCL can pass through the polarizer. The red curves correspond to the cases when the polarizer is at 45º and mainly the light from the left QCL can pass through. As it is shown, the power from the left and right QCL can be tuned rather independently.

5. The Vernier effect of the system

As mentioned above, the system favors the longitudinal modes of the individual QCL cavity that gain maximum external injection. Fig. S5(a) plots the longitudinal modes of the individual laser (upper blue curve) and the injection efficiency through the half racetrack structure (lower red curve), obtained by 3D full-wave simulations using Lumerical FDTD. The longitudinal modes that coincide the peaks of the injection efficiency will be excited. This mechanism determine the mode spacing of the device. As it is shown, the calculation and the experimental result matches well. It is worth noting that the final mode spacing is not equal (96 GHz and 71 GHz), this is due to the waveguide dispersion which makes the original peaks of the blue and red curves not equally spaced.

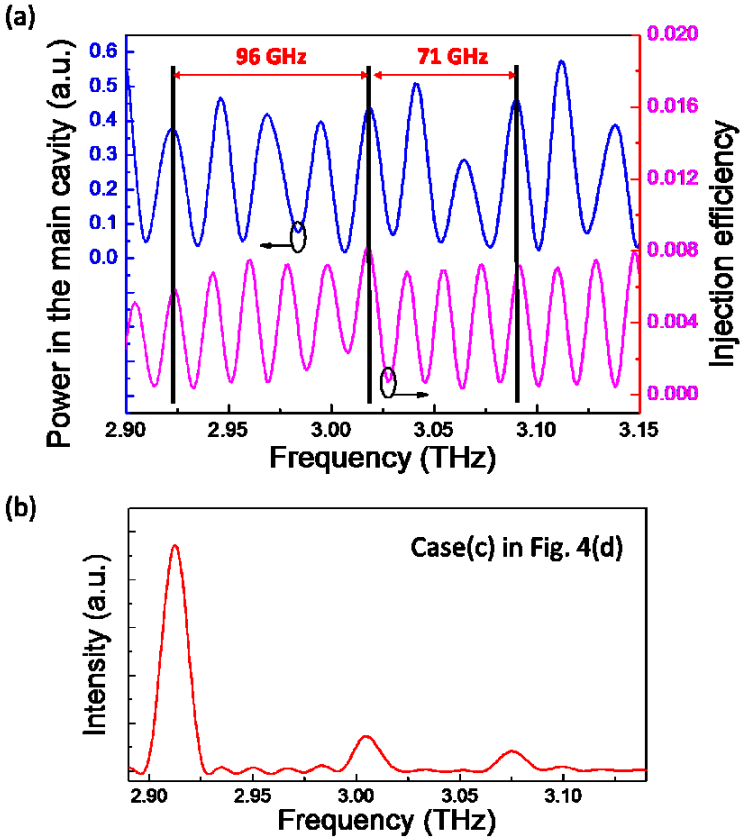

Figure S5. (a) Calculated optical modes in the individual laser cavity (upper blue curve) and the injection efficiency thought the half racetrack structure (lower red curve). (b) Measured spectrum of the device (replot of the curve in Fig. 4(d) of the main text).

6. Schematic illustrations of the fabrication process

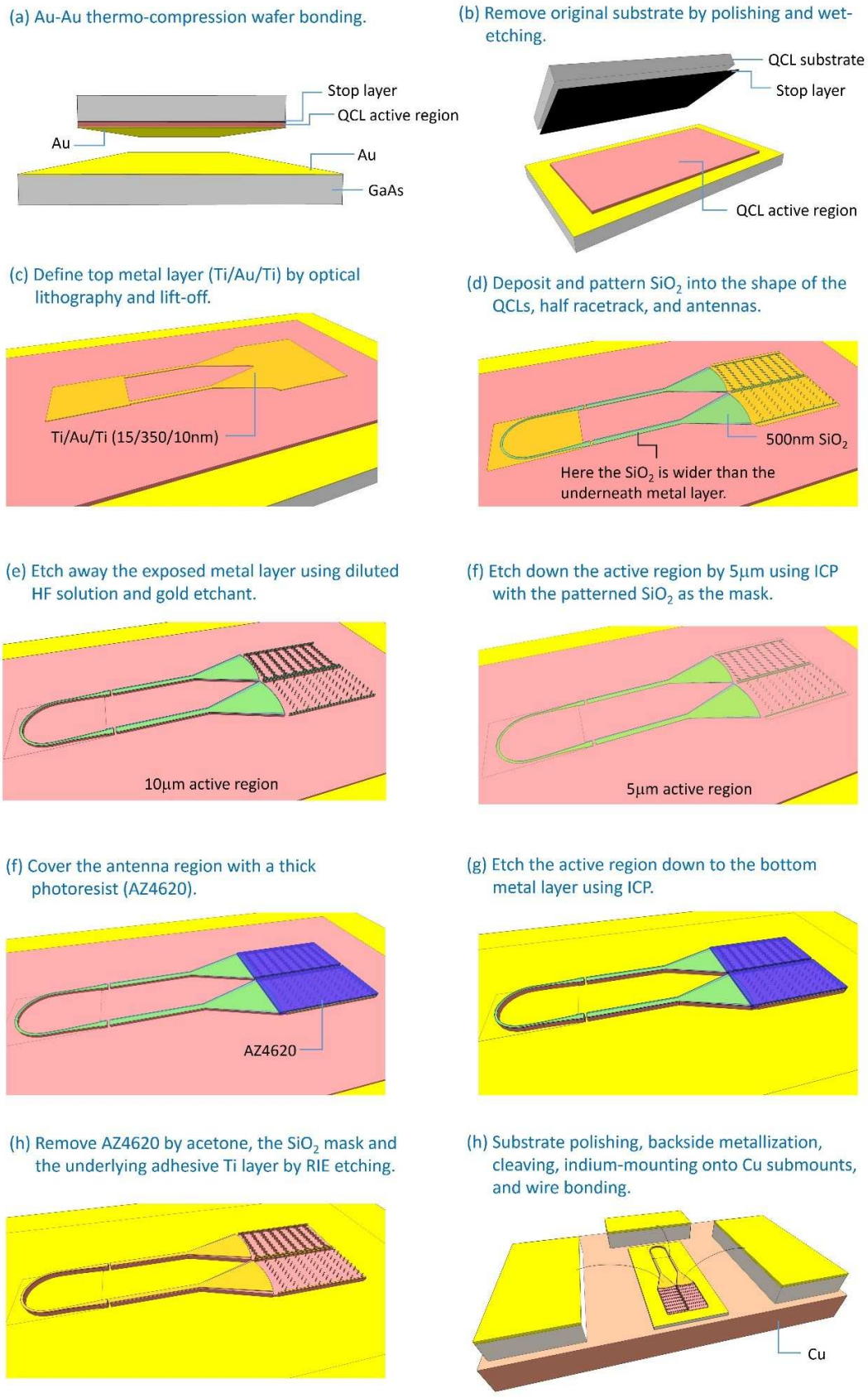

Figure S6. Schematic illustrations of the fabrication process.